Proceedings of ASME Turbo Expo 2011
GT2011
June 6-10, 2011, Vancouver, British Columbia, Canada

GT2011-45150

HEAT TRANSFER, HYDRODYNAMICS AND PRESSURE DROP IN THE MODEL OF A BLADE LEADING EDGE CYCLONE COOLING

Artem A. Khalatov,
Igor I. Borisov,
Sergey D. Severin
Institute for Engineering Thermophysics,
Ukrainian National Academy of Science
Kyiv City, Ukraine

Vyacheslav V. Romanov,
Vladimir Y. Spitsyn,
Yuriy Y. Dashevskyy
Gas Turbine Research & Production Complex
"Zorya"-"Mashproekt"
Mykolaiv City, Ukraine

ABSTRACT

The heat transfer, hydrodynamics and pressure drop have been studied experimentally at the air swirling flow in the round tube with 90^0 exit bend, simulating the blade cyclone cooling. The flow was supplied into the test section from the closed circular plenum through one or two tangential slots (swirl generators) made on the round tube surface. The flow angle to the first swirl generator was 60^0 ($\beta = 0^0$ is the "classic" tangential inlet). The following three configurations, reflecting the actual blade design, were studied, namely: (i) the tube with one swirl generator and open exit, (ii) the tube with one swirl generator and 90^0 exit bend, (iii) the tube with two swirl generators and 90^0 exit bend. The Reynolds number, based on the average axial velocity and tube internal diameter was ranged from 40000 to 105000.

The surface streamline swirl flow angle, static and total pressure excess, heat transfer and pressure losses in the round tube, swirl generator area and exit bend were measured. In terms of the heat transfer rate the best results has demonstrated the configuration with one swirl generator and 90^0 exit bend.

INTRODUCTION

Very limited number of techniques is now in use to cool internally gas turbine blades. They include the impingement cooling, pin fins, continuous and broken ribs, lattice cooling. The potential of these techniques is close to their thermophysical limit, therefore the further increase in the cooling rate may be achieved either by increase in the air flow rate through the blade inner cavity, or via decrease in the cooling channel diameter leading to the dirt blockage problems.

Despite the evident progress in convective cooling systems, there is a necessity to develop alternative cooling techniques, providing the higher heat transfer rate at acceptable pressure losses and relatively simple production technology, which allow avoiding small size features manufacturing in the cooling area. Amongst the other advanced cooling techniques, which are now under consideration, the cyclone cooling, based on the swirl flow concept, looks as promising internal cooling technique [1,2].

In all known cyclone cooling configurations the classic tangential inlet is employed to generate the swirling flow [1-5]. The cylindrical [1, 3 – 5], triangular [6] and square [7] cross section ducts were investigated to assess the passage shape factor. In papers [1], [4] the air into the cyclone chamber supplied tangentially ($\beta = 0^0$) from the plenum through the long slot (length–to–diameter ratio is 18.7 in [4] and is 8.5…26 in [1]). In paper [3] along with traditional flow supply ($\beta = 0^0$) the effect of flow angle ($\beta = 30^0$; 60^0) was also investigated. At the traditional tangential inlet the formation and development of swirling flow is completed at the distance of three passage diameter downstream of the swirl generator edge [8] accompanied with relatively high pressure losses in swirler due to the flow turn.

As shown in [8, 11] the swirl flow circumferential uniformity is established at $x/d > 3.0$ where heat transfer depends on the Reynolds number Re_d and swirl flow parameter - either the total Φ^*(ratio of rotational momentum to the axial flow momentum) or the local one ($\mathrm{Tan}\,\varphi_w$). Here φ_w is the surface streamline swirl flow angle.

As found in [8, 11] for various boundary conditions there is a one-valued correlation between Φ^* and $\mathrm{Tan}\varphi_w$, swirl flow parameters. As the φ_w magnitude is easier measured in experiments, it is more often used in heat transfer and hydrodynamics data processing

The swirling flow decay in an open round tube is described by the exponential correlation [3]:

$$\Phi^* = \Phi_0^* \exp\left(-0{,}04\frac{x}{d}\right) \qquad (1)$$

The multiplication approach described and grounded in [8, 9] is usually used to describe the heat transfer data. According to this approach, the general heat transfer correlation looks as follows:

$$\mathrm{Nu} = \mathrm{Nu}_0(\mathrm{Re})\,\varepsilon_{\varphi T} \qquad (2)$$

Here $\varepsilon_{\varphi T}$ is the swirling flow function depending on the φ_w ; Nu_0 is the reference Nusselt number (fully developed axial turbulent flow in a smooth tube). For the average heat transfer in a round tube the swirl flow parameter is described by the correlation [3]:

$$\varepsilon_{\varphi T} = (1+\Phi^*)^{1{,}75} \qquad (3)$$

The review has shown the only published paper dealing with actual turbine blade supplied with a cyclone cooling in the leading edge area [10] is available now. The coolant (air) is supplied to the cooling chamber through the set of tangential slots. As revealed, the blade rotation does not destroy the swirling flow structure. To take into consideration the Coriolis force influence, the swirling flow direction must have the same direction as a blade rotates.

The review has also shown that in some cases the experimental data obtained in the cyclone cooling model is different to that available in the actual turbine blade. This can be explained by the influence of some internal blade design features, such as distribution of tangential slots, their size, flow and geometric conditions at the cooling passage inlet and outlet.

To apply cyclone cooling technique, very important is knowledge of data on swirling flow structure and pressure losses. Unfortunately this data is unavailable in most published papers, therefore providing the difficulty in the thermal hydraulic performance evaluation. The other problem is very limited data on the pressure losses and heat transfer in the area of swirl generator.

Therefore the objective of this paper is the experimental study of heat transfer, hydrodynamics and pressure losses in the improved cyclone cooling configuration that includes some important the actual blade features. The inclined tangential flow swirl through one or two tangential slots reflects the coolant supply into the blade space, while 90^0 flow bend at the passage exit simulates the coolant discharge into the blade trailing edge area. Based on the heat transfer and pressure drop measurements, the Reynolds analogy factor was found and comparison with typical trip strip rib turbulators was performed.

NOMENCLATURE

Symbols:

B	ambient pressure
d	tube inner diameter
f	pressure drop coefficient;
F	cross-section area;
G	mass flow rate;
h	heat transfer coefficient;
l	tube length;
P	static pressure;
ΔP	static pressure difference;
q	heat flux;
r	radial coordinate;
R	tube inner radius;
	heat flux sensor thermal resistance;
s	swirl generator height;
T	temperature;
t	surface swirl flow pitch;
$\mathrm{Tan}\varphi_w$	local swirl flow parameter,
w	velocity;
x	axial distance;
$Re_d = \frac{wd}{\nu}$	Reynolds number;
$Nu_d = \frac{hd}{\lambda}$	Nusselt number

Greek Symbols:

β	inlet "geometric" flow angle (Fig. 2);
$\varepsilon_{\varphi T}$	swirl flow function (heat transfer);
ν	air kinematic viscosity;
ρ	air density;
ζ	hydraulic resistance coefficient;
φ_w	surface streamline swirl flow angle;
φ_{W0}	surface streamline swirl flow angle at x = 0;
Φ^*	total swirl flow parameter

Subscripts:

bend	exit bend;
d	based on the tube diameter;
g	for heat flux sensor;
s	for swirl generator;
st	static parameters;
w	tube wall;
0	fully developed turbulent flow in a smooth tube.

Superscripts:

$\overline{}$	averaged in the axial direction;
*	based on the total parameters.

EXPERIMENTAL FACILITY & PROCEDURE

The test rig schematic view for the hydrodynamic or heat transfer studies is given in Fig. 1. The room air from the blower 1 is supplied into the test section 5 through the flow meter 2, plenum (flow distributor) 3 and electric heater 4. The hydrodynamic study was performed at the room flow temperature, while the heat transfer studies were carried out at the wall-to-air heat flux. Two test sections of the identical geometry were made, one of them for the hydrodynamic experiments, while the other one for the heat transfer studies.

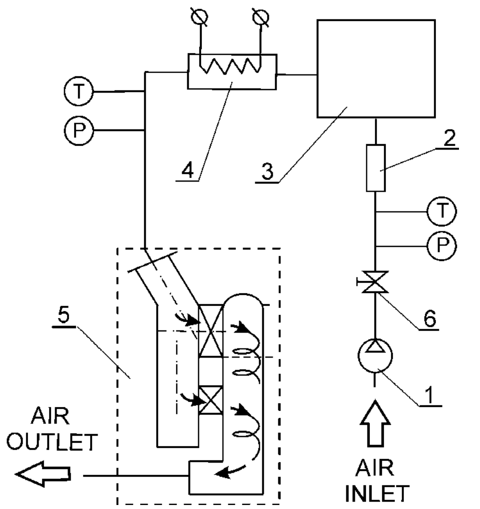

Fig. 1 Test rig schematic view. 1 – blower; 2 – flow meter; 3 – plenum; 4 – electric heater; 5 – test section (two swirl generators); 6 – valve.

The Figure 2 presents the test section layout, corresponding to an actual blade design [11] (scale is 5:1). The inlet boundary conditions include geometric angle $\beta = 60^0$, the outlet boundary conditions include 90^0 exit bend. The experiments can be performed with an open exit, 90^0 exit bend and one or two distributed swirl generators.

Hydrodynamic measurements. The round tube (Fig. 2) designated for the hydrodynamic studies was made of the transparent and polished acrylic. The test section provides investigation of different cyclone cooling configurations, including open tube exit, 90° exit bend, one or two swirl generators. The tube (cyclone chamber model) basic geometric parameters are: (i) one swirl generator: the inner diameter d is 20 mm, passage length l is 240 mm ($l/d = 12$); (ii) two swirl generators: d is 20 mm, l is 260 mm ($l/d = 13$).

The distributor length is 200 mm. The tangential slot height s is 5.0 mm for both swirl flow configurations the axial slot length is 59 mm for the first swirl generator and 23.5 mm for the second one. Distance between slots is 98.5 mm. The second slot length was taken after preliminary testing to provide the mass flow ratio between two swirl generators as 7:3. This distribution is close to the actual flow conditions and was actually constant for all Reynolds numbers.

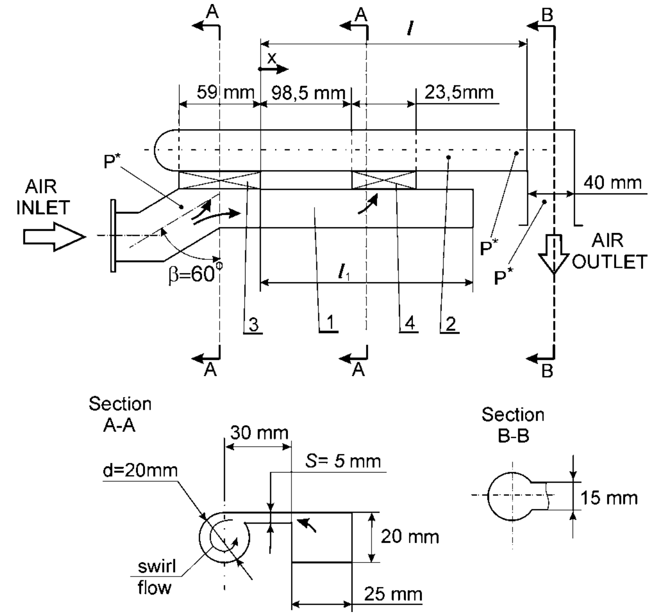

Fig. 2 Test section layout. 1 – flow distributor; 2 – test section (for two swirl generators); 3 – swirl generator #1; 4 – swirl generator #2.

To provide the wall static pressure measurements several holes were drilled in the test section wall. Also two holes (0.8 mm in a diameter) close to each slot edge were made to provide the surface spiral streamline visualizations due to the color water injection.

The following basic parameters were measured in the experiments: total air flow rate, air flow rate through the swirl generator #2, wall static pressure at four points of the test section, total and static pressure inside swirl generator # 2, total and static pressure in the distributor - in front of the swirl generators #1 & #2, total pressure after 90^0 exit bend, in-tube radial total pressure field, surface streamline swirl flow angle (visualizations), air flow temperature at the test section inlet. The total and static pressures were measured by means of the Pitot tube, the radial total pressure field- by the total pressure sensor at the test section end ($x/d = 14$).

The mass flow rate through the swirl generator #2 was measured using the total pressure probe placed inside the swirl generator, as well as the static pressure and temperature in front of the swirl generator. The probe was tested using precise flow meter SMC PF2A703H. The air mass flow rate through the swirl generator #1 was calculated as the difference between total mass flow rate and mass flow rate coming through the swirl generator #2.

The surface streamline swirl flow angle was determined based on the spiral streamline visualization on the inner surface of the test section. To do this the color water was injected into the swirling flow. The measurements of the surface spiral line pitch *t* allowed us to determine the surface streamline swirl flow angle using the correlation $\varphi_w = \text{arc Tan } (\pi d/t)$, where d is the tube internal diameter.

The pressure drop coefficient was calculated based on the wall static pressure excess measurements (ΔP_w) as they are nearly equal to the average total pressure excess at the same *x* coordinate. This experimental fact was revealed in the open tube with axial blade swirl generator [8] and was confirmed in this study for the inclined-tangential flow swirl and flow exit bend.

The hydraulic resistance coefficient for the swirl generator was determined according to the following correlation:

$$\zeta_S^* = \frac{\Delta P^*}{\rho_S w_S^2 / 2} \quad , \qquad (4)$$

where ΔP^* is the total pressure difference, measured in front of the swirl generator (in the distributor) and in the tube cross section directly after the swirl generator; w_S, ρ_S is the averaged air speed and air density in the swirl generator slot.

The density ρ_S was determined based on the inlet static pressure and temperature measurements. The average air speed in the swirl generator slot was determined according to the following correlation:

$$w_S = \frac{G_S}{F_S \rho_S} \quad , \qquad (5)$$

where G_S is the air mass flow rate through the swirl generator, F_S is the swirl generator cross section area.

The hydraulic resistance coefficient of the exit bend was found from the correlation:

$$\zeta_{bend}^* = \frac{\Delta P_{bend}^*}{\rho_{bend} w_{bend}^2 / 2} \quad , \qquad (6)$$

where ρ_{bend}, w_{bend} is the air average density and flow average axial velocity in front of the bend.

The in-tube pressure drop coefficient was found according to the correlation:

$$f = \frac{\Delta P^*}{\frac{1}{d}\frac{\rho w^2}{2}} \quad , \qquad (7)$$

where $\Delta P^* \approx \Delta P_w$, ΔP_w is the wall static pressure excess; ρ is the average air density; w is the averaged axial speed in the tube cross section:

$$w = \frac{G}{\rho F} \qquad (8)$$

All comparisons were made using the reference pressure drop coefficient f_0 in the round smooth tube at the fully developed turbulent flow (Blasius correlation):

$$f_0 = \frac{0.3164}{Re_d^{0.25}} \qquad (9)$$

Here the Reynolds number is based on the average axial velocity and tube internal diameter:

$$Re_d = \frac{wd}{\nu} \qquad (10)$$

Heat transfer measurements. The test section of the same geometry as for the hydrodynamic studies was used in the heat transfer experiments. To provide the measurements the test section was assembled from seven separate copper cylindrical sections with individual jackets through which the cooling water was pumped.

The following basic parameters were measured: total air mass flow rate, air flow rate through the swirl generator #2 (case with two swirl generators), tube inner wall temperatures in four points, air flow temperatures in front of the heater, in the distributor, inside the swirl generators #1 & #2, as well as at the test section outlet. The local heat flux in separate tube points; average heat flux within the swirl generator area by means of the calorimetric technique was also measured.

The air flow temperature and the tube wall temperatures were measured by means of K-type thermocouple, the outlet air average temperature was measured by the electronic digital thermometer. For the configuration with exit bend this temperature was measured in the exit tube just after the exit bend. To provide average temperature measurements, the electronic digital thermometer was placed into the insulated closer, where the air flow from the test section outlet sucked to by means of the vacuum pump.

Local surface heat fluxes were measured by micro-foil heat flux sensors RdF # 20450–1. The nominal sensors sensitivity is 0.005...0.006 $\mu V/(W/m^2)$, response time is 0.4 s, thermal resistance R is 0.0005 $K/(W/m^2)$. All sensors are of 8x13 mm^2 in size, the sensor axial coordinate corresponds to the sensor center. The heat flux was considered as being uniform in the angular direction. At the edge of swirl generator #1 the heat flux was measured by means of the heat flux sensor RdF # 27036-3.

All heat flux sensors were glued onto the tube inner surface, to provide appropriate tube smoothness all gaps were filled in with a sealant having approximately the same heat conductivity. Signals from all sensors were registered by the precise micro–voltmeter.

The total heat fluxes in the areas of swirl generators #1 and #2 were measured using the calorimetric technique. For this purpose, the water mass flow rates through each swirl generator cooling area were measured along with the water temperature differences in the cooling areas. These measurements were made by the K-type thermocouples.

The heat transfer coefficient was determined according to the following correlation:

$$h = \left(\frac{\Delta T}{q_g} - R \right)^{-1} \quad , \qquad (11)$$

where $\Delta T = T_f - T_w$ is the temperature difference between the averaged flow temperature at the x distance and local copper tube temperature; q_g is the heat flux coming through the sensor; R is the heat flux sensor thermal resistance.

As the measured heat flux is different to the actual heat flux due to the sensor thermal resistance, then the iteration procedure was developed to process experimental data. As a first approach, the measured q_g magnitudes were approximated to develop the appropriate correlation. The obtained correlation was integrated from the initial section (x = 0) to the point of measurement to recalculate the local heat flux and average flow temperature in each measurement point. The found magnitudes were used to find the heat transfer coefficient via the correlation 11 and improved heat flux according to the correlation:

$$q = h \cdot \Delta T \qquad (12)$$

This procedure was repeated up to the acceptable procedure convergence was reached. As a result, the heat flux and flow temperature distributions were obtained and the heat transfer coefficient was determined. This approach was also used in the preliminary testing with axial in-tube flow.

The heat transfer augmentation rate was determined using the reference correlation for the fully developed turbulent axial flow in the round smooth tube (Dittus-Boelter correlation):

$$Nu_0 = 0.023 \cdot Re_d^{0.8} \cdot Pr^{0.4} \qquad (13)$$

All comparisons in terms of the Nusselt number ratio (Nu/Nu_0) were made at the identical Reynolds number.

Experimental uncertainty. The standard uncertainty procedure was used as recommended by Coleman and Steele [12]. Using the uncertainty of 0.1 mm for all dimensions of the test section, 0.5^0 for all temperatures and ± 1% for all air physical properties, the maximum relative uncertainties of the mass flow rate and Reynolds number was estimated as ± 2.8% and ± 3.0%, respectively. The maximum uncertainty of the static pressure difference was estimated as ± 2.0%, while the overall maximum relative uncertainty of the pressure drop coefficient was determined as ±3.8%. The maximum relative uncertainties of the specific heat flux, temperature difference and average heat transfer coefficient was ±10%, ±3.5% and ±10.6% respectively, giving the maximum relative Nusselt number uncertainty of ±10.8%. All uncertainties are expressed with 95% confidence.

RESULTS AND DISCUSSION

As mentioned, three cyclone cooling configurations were studied, including (i) the tube with one swirl generator and open exit, (ii) tube with one swirl generator and 90° exit bend, (iii) tube with two swirl generators and 90° exit bend.

The basic flow parameters used in the experimental program were as follows: air mass flow rate ranged from 0.008 to 0.035 kg/s; Reynolds number ranged from 40000 to 105000; major experimental measurements were made at Reynolds number ranging from $9 \cdot 10^4$ to 10^5; inlet flow temperature in the hydrodynamic experiments was 20°C, while in the heat transfer experiments it was changed from 90^0C to 105°C.

In all experiments the test section beginning (x = 0) was calculated from the swirl generator #1 edge. For the configuration with two swirl generators the Reynolds number was based on the total air flow rate coming through both swirl generators.

Total pressure

The radial total pressure excess distribution in the tube with one swirl generator is shown in Fig. 3 (x/d=14.0; Re_d = 90000; open tube; 90^0 exit bend). The total pressure changes significantly in the radial direction and some flow asymmetry can be observed.

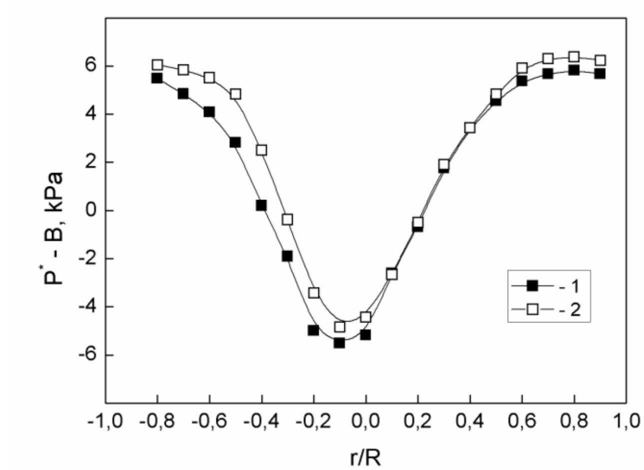

Fig. 3 Radial distribution of the total pressure excess, x/d = 14. One swirl generator, Re_d = 90000. 1 – open exit; 2 – 90^0 exit bend.

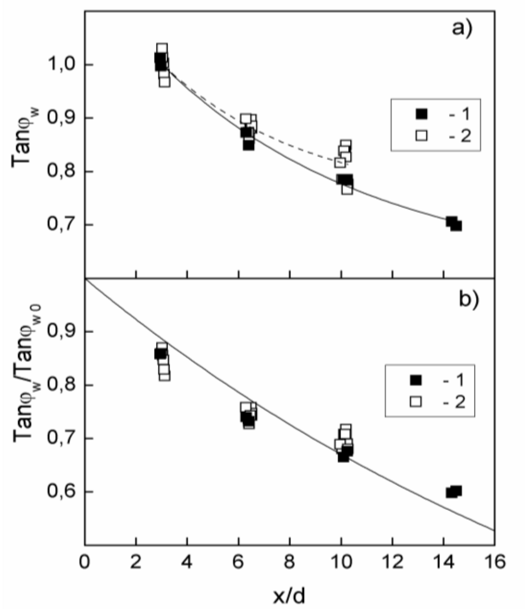

Fig. 4 Axial distribution of the surface streamline swirl flow angle. One swirl generator. 1 – open exit; 2 – 90^0 exit bend; the line in the Fig. 4b is according to [3].

The processing of this data has shown the averaged excess total pressure is in a good agreement (±3%) with excess wall static pressure at the same axial distance. The same conclusions were obtained in the test section with two swirl generators. In this case the measurements were made at the non- dimensional distance x/d of 1.2 downstream the swirl generator # 2 (Re_d = 100000).

Flow swirl

The axial distribution of surface streamline swirl flow angle is given in Fig. 4. Due to the flow rearrangement in front of the exit bend, the Tan φ_w magnitude is slightly greater (5%) then that occurred in the tube with open exit (Fig. 4.a). Approximation of Fig. 4.a data shows the initial surface streamline angle is about 49^0 ($Tan\varphi_{W0}$ is 1.15) for both cases (geometric inlet angle is 90 - β = 30^0). The non-dimensional surface streamline flow angle for the scheme with one swirl generator (Fig. 4.b) corresponds to the correlation, presented in [3], where other boundary conditions and Reynolds number range were studied.

The data regarding the average surface streamline swirl flow angle $\overline{\mathrm{Tan}\,\varphi_W}$ is shown in Fig. 5. In the tube with one swirl generator the magnitude of $\overline{\mathrm{Tan}\varphi_W}$ ranges from 0.9 to 0.95 for all Reynolds numbers studied, while the exit boundary conditions (open exit or exit bend) influence the $\overline{\mathrm{Tan}\,\varphi_W}$ distribution weakly. For the tube with two swirl generators (Fig. 5.b) in the area between swirl generators the $\overline{\mathrm{Tan}\,\varphi_W}$ magnitude is around 1.4 for all Reynolds numbers, while after swirl generator #2 it is only 1.1.

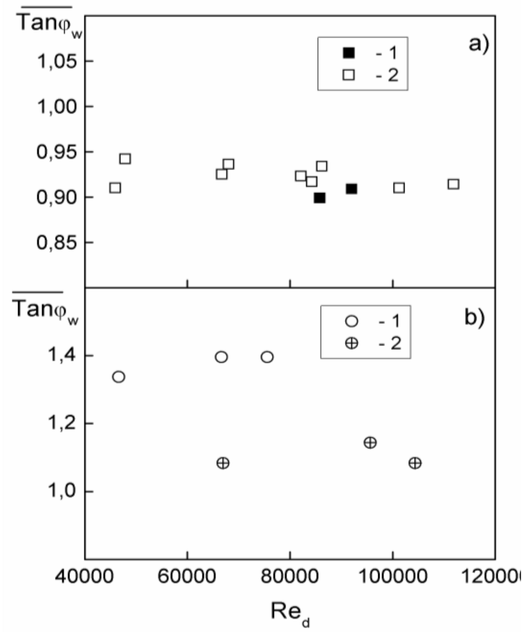

Fig. 5. Averaged surface streamline swirl flow angle. a) one swirl generator: 1 – open bend, 2 – 90^0 exit bend; b) two swirl generators and 90^0 exit bend: 1 – area between swirl generators, 2 – area between swirl generator # 2 and exit bend.

Pressure drop

As mentioned, all pressure drop coefficients and hydraulic resistance coefficients (correlations 4, 6 & 7) are based on the average excess total pressure drop, calculated as the excess wall static pressure drop. Data regarding the test section, swirl generator area and exit bend are presented in Fig. 6.

Test section. For both schemes with one swirl generator (Fig. 6.a) the axially averaged pressure drop coefficient is summarized by the following correlation:

$$\bar{f} = 2.16 \cdot Re_d^{-0.25} \qquad (14)$$

For the scheme with two swirl generators the pressure drop coefficient is almost constant for all Reynolds numbers.

For the scheme with one swirl generator the average pressure drop factor $\bar{f}/f_0$ is around 7.0, whereas for the scheme with two swirl generators it is about 5.0. Thus, the scheme with two swirl generators provides the average magnitude of $\bar{f}/f_0$ lower by 30%.

Swirl generators. The hydraulic resistance coefficient ζ^*_{S1} for the swirl generator #1 is shown in Fig. 6.b. This coefficient is about 3.0 and is almost independent on the Reynolds number for both schemes. For the swirl generator #2 the pressure drop coefficient ζ_{S2} is 3.75 and is constant in the whole Reynolds number range.

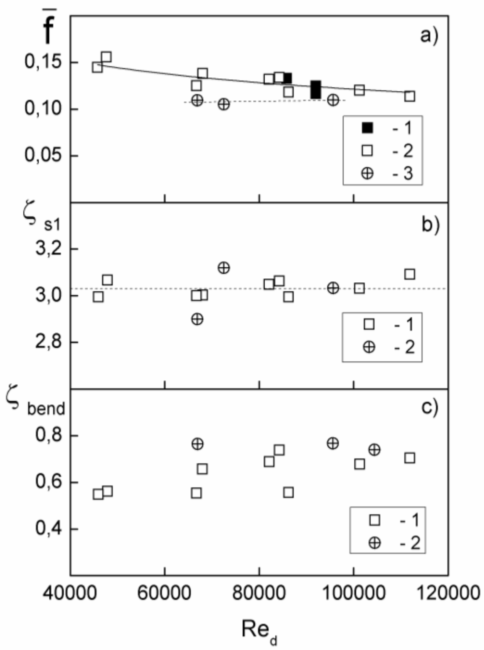

Fig. 6 Pressure drop and hydraulic resistance coefficients. a) axially averaged pressure drop coefficient. 1 – one swirl generator, open exit; 2 - one swirl generator, 90 ^{0} exit bend; 3 – two swirl generators, 90 ^{0} exit bend; b) swirl generator # 1; c) exit bend; 1, 2 – one or two swirl generators.

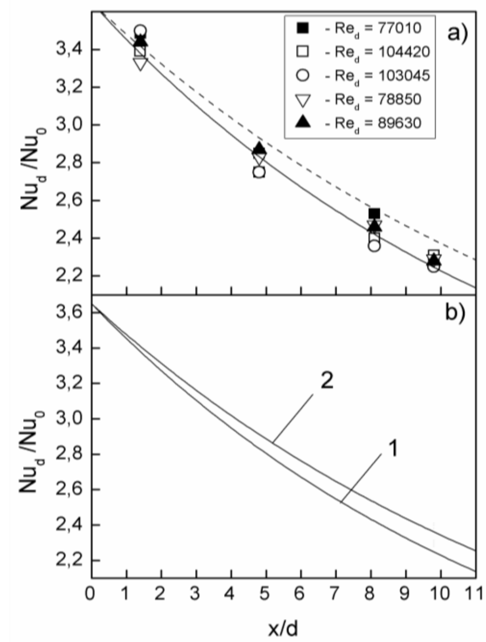

Fig. 7 The Nu/Nu$_0$ ratio axial distribution. a) one swirl generator, open exit; dotted line is based on the correlation (3). b) experimental data: one swirl generator; 1 – open exit; 2 – 90 ^{0} exit bend.

Exit bend. Fig. 6.c represents the hydraulic resistance coefficient in the exit bend. For the scheme with one swirl generator the pressure drop coefficient is growing slightly to reach value of 0.65…0.7 at Reynolds number of 100000. For the scheme with two swirl generators the value of ζ^*_{bend} is 0.75 for all Reynolds numbers studied.

Note that hydraulic resistance coefficient at the axial flow through the bend was also measured for comparisons. This coefficient was around 1.0, i.e. by 30% greater of that at the swirling flow. This important fact can be explained by more favorable flow conditions for the swirling flow inside the exit bend.

Local heat transfer

Figure 7.a shows the heat transfer enhancement rate for the scheme with one swirl generator (Nu_0 was based on the correlation 13). Here the solid line describes the experimental data obtained in this study. As seen, variations in the Reynolds number from 77000 to 104000 influence the Nu_d/Nu_0 ratio weakly. The dotted line is the correlation (3), based on the initial surface swirl flow angle ($\varphi_{W0} = 49^0$), found in the present study.

As found, the experimental data obtained in the tube with open exit is well described by the following exponential correlation (normalized Nusselt number):

$$\frac{Nu_d}{Nu_0} = 1 + 2.65\exp\left(-\frac{x/d}{13.0}\right) \qquad (15)$$

Figure 7.b presents comparison of heat transfer enhancement rate for two schemes with open exit and exit bend. The exit bend influences the upstream swirl flow and leads to the flow rearrangement in the axial and tangential directions. Also, the exit bend provides a certain heat transfer enhancement, this phenomenon is more appreciable in the second portion of the tube. The experimental data scattering in the initial tube area may be explained by some angular flow non-symmetry.

The axial distribution of heat transfer augmentation rate in the tube with exit bend is well summarized by the following exponential correlation:

$$\frac{Nu_d}{Nu_0} = 1 + 2.65\exp\left(-\frac{x/d}{14.7}\right) \qquad (16)$$

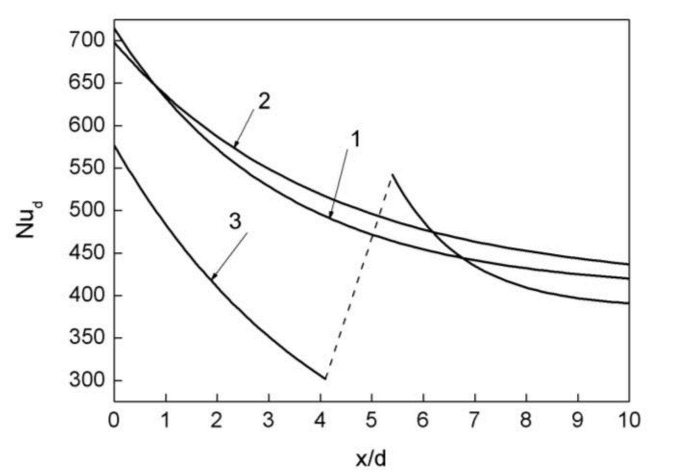

Fig. 8 The Nusselt number axial distribution, $Re_d = 100000$.

1 – one swirl generator, open exit; 2 – one swirl generator, 90 ^{0} exit bend; 3 – two swirl generators, 90 ^{0} exit bend.

Figure 8 gives comparison of local Nusselt numbers for the configurations with one and two swirl generators at Reynolds number of 100000. As seen, the heat transfer rate in the tube with one swirl generator (both cases) is greater then that obtained in the tube with two swirl generators.

Despite relatively high surface streamline swirl flow angle in the area between swirl generators, the lower heat transfer rate here can be explained by the lower air mass flow. Downstream the swirl generator #2 the negative effect on the heat transfer rate is due to the mixing of hot and cold air within the second swirl generator area. The eddy structure formation was occurred after the swirl generator # 2 as a result of energy dissipation due to the mixing of two swirling flows of different intensity. This phenomenon is also discussed in [13]. As a whole, heat transfer rate in the tube with one swirl generator is by 20% greater of that occurred in the tube with two swirl generators.

Average heat transfer

Figure 9 illustrates axially averaged Nusselt number versus Reynolds number for all configurations studied. At $Re_d >$ 80000 the greatest heat transfer rate demonstrate configurations with one swirl generator, while the lowest one shows configuration with two swirl generators. Data for one swirl generator is in a good agreement with data [4], obtained in the test section with two swirl generators and 90 ^{0} radial exit slot.

Thermal performance

The thermal performance analysis was carried out based on the Reynolds analogy factor $\frac{Nu_d / Nu_0}{f / f_0}$ for the test section with swirling flow, as well as for the whole passage including pressure drop and heat transfer in the swirl generator #1. The calculated magnitudes Reynolds analogy factor data versus

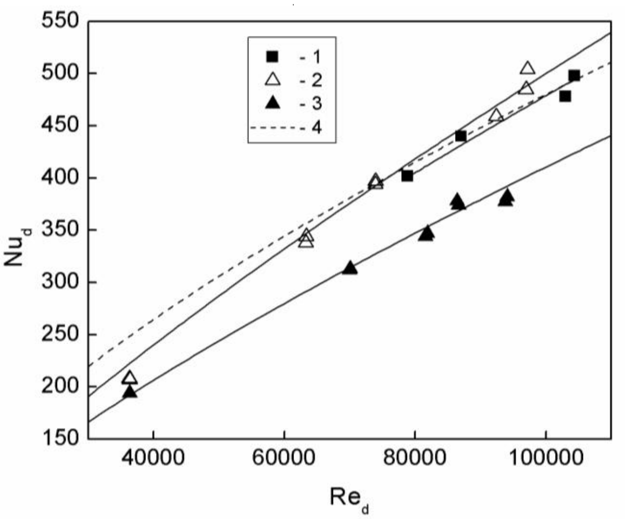

Fig. 9 The averaged Nusselt number. 1 – one swirl generator, open exit; 2 – one swirl generator, 90 ^{0} exit bend; 3 – two swirl generators, 90 ^{0} exit bend; 4 – two swirl generators, radial exit slot [4]

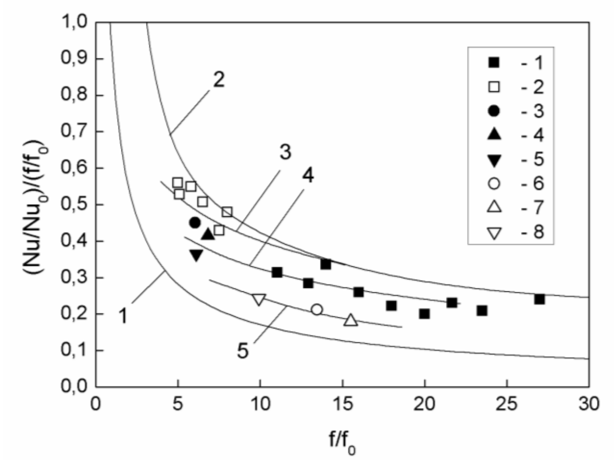

Fig. 10 The Reynolds analogy factor versus non-dimensional pressure drop factor

Lines: 1 – transverse rib turbulators at high Reynolds numbers (square cross section) [15]; 2 – surface dimples at low Reynolds numbers [14]; 3, 4 – swirling flow, open exit and exit tangential slot [5]; 5 –numerical simulation; round passage, trip strip turbulators [16]: continuous V–shaped ribs, broken V–shaped ribs, continuous helical ribs.

Symbols: 1, 2 – swirling flow in square cross section passage [7]; 1 - single row of holes, 2 - dual row of holes; 3 – 8 : this study; 3, 6 : one swirl generator and open exit (without and including swirl generator #1); 4, 7 : one swirl generator and 90 ^{0} exit bend (without and including swirl generator #1); 5, 8 : two swirl generators and 90 ^{0} exit bend (without and including swirl generators #1 and #2).

relative pressure drop factor is shown in Fig. 10. The following basic conclusions can be extracted from this data analysis:

– data for all configurations are located within the area between two boundary lines, considered in [14]. The lower line (1) describes data for the transverse ribs turbulators at high Reynolds numbers [15], while the upper one (2) belongs data obtained in the dimpled passage at low Reynolds numbers;

– data for the test section without pressure losses and heat transfer inside the swirl generator #1 agrees well with experimental data [7] for the swirling flow in the square cross section passage (single row of inlet holes) and exit bend;

– data including pressure losses and heat transfer in the area of swirl generator # 1 (symbols 6, 7, 8) agrees well with data for the trip strip turbulators of different configurations (continuous V–shaped ribbing, broken V–shaped ribbing and continuous helical ribbing) [15].

CONCLUSIONS

The heat transfer and hydrodynamics have been studied experimentally at the air swirling flow in round tube simulating the cyclone cooling of the turbine blade leading edge area. Unlike the earlier studied configurations a few boundary conditions typical to the actual gas turbine blade were investigated including the inclined-tangential flow swirl and 90^0 exit bend. The following primary conclusions can be drawn from this study results:

- the inlet and outlet boundary conditions influence greatly on the heat transfer, swirling flow structure and pressure losses;
- for the boundary conditions studied, at the identical tube axial distance the averaged total pressure excess is identical to the wall static pressure excess;
- in the tube with one swirl generator the surface swirl flow angle reduces according to the exponential law; the heat transfer rate and pressure drop factor are independent on the Reynolds number;
- in the tube with two swirl generators the heat transfer is reduces slightly in the area between swirl generators, but the rapid growth is immediately after the swirl generator #2;
- the greatest heat transfer rate have demonstrated the configurations with one swirl generator, while the lowest one – the configuration with two swirl generators and 90^0 exit bend;
- for all configurations the Reynolds analogy factor is as good as the continuous V–shaped ribs, broken V–shaped ribs and continuous helical ribs used in the blade gas turbine cooling; however simpler production technology is an inherent advantage of the cyclone cooling configurations.

ACKNOWLEDGEMENTS

This research was supported financially by the Ukrainian National Academy of Sciences. The partial support of the Gas Turbine Research & Production Complex "Zorya"-Mashproekt" (Mykolaiv City, Ukraine), Grant #298 is also acknowledged.

REFERENCES

[1] Glezer B., Moon H.K., O'Connel T. *A novel technique for the internal blade cooling //* ASME Paper № 96–GT–181.

[2] Harvey N.L., Ireland P.T., 2008, *Cooling of gas turbine engine aerofoils* // U.S Patent №77399160 - F01D 5/18.

[3] Hay N, West P.D., 1975, *Heat Transfer in Free Swirling Flow in Pipe // Heat Transfer*, pp. 100–106.

[4] Hedlund C.R., Ligrani P.M., 2000, *Local swirl chamber heat transfer and structure at different Reynolds numbers // Journal of Turbomachinery*, Vol. 122.- pp. 375-385.

[5] Khalatov A., Syred N., Bowen P., et al., 2000, *Innovative Cyclone Cooling Scheme for Gas Turbine Blade: Thermal-Hydraulic Performance Evaluation* // ASME Paper № GT2000-237.

[6] Hwang J.J., Cheng C.S., 1999, *Augmented heat transfer in a triangular duct by using multiple swirling jets // Journal of Heat Transfer*. Vol. 121, No. 3. – P. 683–690.

[7] Ekkad S.V., Pamula G., Acharya S., 2000, *Influence of crossflow-induced swirl flow and impingement on heat transfer in an internal coolant of a turbine airfoil // Journal of Heat Transfer,* Vol.122, №3.-pp.587-597.

[8] Khalatov A.A., 1989, *Swirl Flows: Fundamentals and Applications,* Kiev, Ukraine, Naukova Dumka (in Russian).

[9] Shchukin V.K., Khalatov A.A., 1982, *Heat transfer and hydrodynamics of the swirling flows in axisymmetric passages*, Mashinistroenie (Publisher), Moscow (in Russian).

[10] Glezer B., Moon H.K. et al. *Heat transfer in rotating radial channel with swirling interal flow //* ASME Paper № 98–GT–214.

[11] Khalatov A. et al. *Gas Turbine Blade with Internal Cyclone Cooling of Leading Edge* // Patent of Ukraine No49125, 2010

[12] Coleman H., Steele G., 1999, *Experimentation and uncertainty analysis for engineers,* John Wiley & Sons, New York, NY, 2d Edition, 275 p.

[13] Harvey N.L., 2006, *Cooling of gas turbine engine aerofoils* // Patent of United States №7137781- F01D 5/18.

[14] Khalatov A.A., Onishchenko V.N., Borisov I.I., 2007, *Analogy of Heat Transfer and Quantity of Motion in the Passages with Surface Vortex Generators* // Reports of Ukraine National Academy of Sciences, No.6., pp.70-75 (in Russian).

[15] Haasenritter A., Weigand B. *Optimization of the rib structure inside a 2D cooling passage* // ASME Paper GT2004–53187. – 10 p.

[16] Khalatov A.A., Dashevskyy Y. Y., Pis'mennyi D.N., 2010, *Rib Configuration Influence on the Heat Transfer and Pressure Drop in a Blade Leading Edge Cooling Passage* // Promyshlennaya Teplotechnika, Vol.32, No4, pp.54–62.